Journal of
Composites Science

MDPI

Article

Mechanical Properties of Dispersion-Strengthened Iron-Based W+WC(Ni) Composite Produced by Combined Wire Electron-Beam Manufacturing with Powder Addition

Andrey Vorontsov [1], Anna Zykova [1], Denis Gurianov [1], Nikolay Shamarin [1], Aleksandr Panfilov [1], Andrey Chumaevskii [1], Kirill Kalashnikov [2,*], Evgeny Kolubaev [1] and Nikolai Savchenko [1]

[1] Institute of Strength Physics and Materials Science of the Siberian Branch of the Russian Academy of Sciences, pr. Akademicheskii, 2/4, 634055 Tomsk, Russia; vav@ispms.ru (A.V.); zykovaap@mail.ru (A.Z.); desa-93@mail.ru (D.G.); shnn@ispms.ru (N.S.); alexpl@ispms.ru (A.P.); tch7av@ispms.ru (A.C.); eak@ispms.ru (E.K.); savnick@ispms.tsc.ru (N.S.)
[2] Department of Engineering, University of Palermo, Viale delle Scienze, 90128 Palermo, Italy
* Correspondence: kirill.kalashnikov@unipa.it

Abstract: The paper investigates the microstructure and mechanical properties of a steel matrix composite reinforced with tungsten (W) particles and a mixture of tungsten carbide and nickel (WC(Ni)) obtained by a hybrid additive manufacturing method using wire electron beam additive manufacturing with powder addition. The composite exhibits a gradient structure including three zones: a matrix of high alloy steel 401S45, a transition layer with a low concentration of W/WC(Ni) and a surface layer enriched with particles of reinforcing phases. SEM, TEM and XRD methods revealed a heterogeneous microstructure consisting of α-Fe (80 vol.%), γ-Fe (10 vol.%) and carbide phases, as well as suppression of the formation of brittle Me_3C intermetallides due to the controlled diffusion of W, C and alloying elements. The microhardness of the composite increases from 350 HV (matrix) to 650 HV (reinforced layer) due to dispersion hardening and formation of the carbide skeleton. Compression tests showed record strength of the reinforced layer (1720 $\pm$ 60 MPa) due to effective load distribution by W/WC(Ni) particles, but brittle failure is observed in tensile tests due to stress concentration at the interfaces.

Keywords: steel matrix composite; mechanical properties; additive technology; gradient structure; tungsten carbide; phase composition

Academic Editor: Sergio T. Amancio-Filho

Received: 26 February 2025
Revised: 14 March 2025
Accepted: 19 March 2025
Published: 21 March 2025

Citation: Vorontsov, A.; Zykova, A.; Gurianov, D.; Shamarin, N.; Panfilov, A.; Chumaevskii, A.; Kalashnikov, K.; Kolubaev, E.; Savchenko, N. Mechanical Properties of Dispersion-Strengthened Iron-Based W+WC(Ni) Composite Produced by Combined Wire Electron-Beam Manufacturing with Powder Addition. *J. Compos. Sci.* **2025**, *9*, 144. https://doi.org/10.3390/jcs9040144

1. Introduction

Steel matrix composites are formed by incorporating reinforcing materials (such as nitrides, carbides, borides, oxides and intermetallic compounds) into the steel matrix, which allows the manufacturing of materials with enhanced performance characteristics [1–5]. Synthesis of such composites is an effective approach to improve the mechanical properties of steel: strength, hardness, fatigue life, and wear resistance [4].

WC is a common ceramic strengthening material that is widely used as a strengthening agent in nickel-based and iron-based alloys [6]. For such materials, WC tungsten carbide is well suited because of its high melting point, thermal stability, strength and hardness, good wettability, and similar thermal expansion coefficient to iron. However, metal-ceramic materials with high hardness cannot be prepared by conventional processing methods. That is why, in recent years, numerous attempts have been made to fabricate WC/Fe,Ni composites using different methods, including additive technologies [2,7–17].

The results of [12] showed that it is possible to produce SS316L-WC stainless steel composite parts using Laser Powder Bed Fusion, Binder Jetting, and Spark Plasma Sintering. It is shown that there is some level of WC dissolution followed by interatomic diffusion occurring between WC inclusions and SS316L matrix, with the final structure and microhardness of the composite system depending on the process kinetics. In [13], Fe-Cr-C-W cladding alloys with a hardness of 37.9HRC were prepared using an additive arc cladding technique with optimized Cr and W content in the powder wire. In this approach, the microstructure of the clad alloys changes from ferrite to martensite, ferrite, residual austenite, carbides and other compounds such as $(Cr,Fe)_7C_3$, WC, Fe_2W, etc. In the study [14], WC particles are used as a hardening phase to compensate for deficiencies in 316L steel. Laser melting deposition was used to prepare 316L samples with different ratios of WC particles. The results show a homogeneous distribution of WC particles in the coating. The microhardness and wear resistance of the 316L/WC composite coating were significantly improved by increasing the WC fraction. The tensile strength and elongation are the best when the WC mass fraction is 6%. In [15], WC-NiCr powder was deposited on 080 M40 steel by Laser Metal Deposition. The results show uniform carbide distribution, stable morphology, and low porosity. In [16], a new, highly wear-resistant WC/18Ni-300 composite was fabricated from a mixture of WC and martensitic steel by selective laser melting. Microstructural analysis shows that the WC particles were partially or completely melted in the SLM process with homogeneous distribution. Moreover, a phase transition from α-Fe to γ (Fe, Ni) appears after the addition of WC reinforcement. In [17], Wire and Arc Additive Manufacturing is applied to produce composite components with a steel matrix by introducing WC/Fe powder into the melt bath by side-feeding the powder under gravity. Maximum strength, microhardness, and minimum wear are achieved in samples with 40, 100 and 80 wt.% WC powder, respectively.

One of the main problems arising in the development of high-performance WC-steel composites is the formation of thick and brittle reaction layers between reinforcing particles and matrix due to the formation of Me_3C carbides [8]. This leads to crack propagation, which subsequently propagates along the WC-steel interface [9]. If this occurs, WC tungsten carbide particles cannot effectively carry the load, which deteriorates the mechanical properties of the composite material. Controlling the phase evolution at the WC-steel interface must depend on the diffusion of tungsten, carbon, iron and other alloying elements, which is extremely difficult due to the non-equilibrium nature of additive technologies associated with large energy input. For WC tungsten carbide particles to provide good bearing capacity, attention must be paid to controlling the thickness of the reaction layer at the WC-steel interface [10,11].

It is known that the nickel and tungsten carbide (Ni-WC) system demonstrates the best performance in the production of high wear-resistant claddings for various tools used in the oil and gas industry [18]. In the Ni-WC system, tungsten carbide particles provide the desired wear resistance, while nickel alloys have relatively high fracture toughness, which neutralizes the embrittlement processes of tungsten carbides [19,20]. Tungsten slows down the kinetics of carbide release in steels due to its slow diffusion [21,22]. In [23], the introduction of tungsten into Cr-Mo-V-doped hot working tool steel results in improved mechanical properties due to the suppression of nanoscale carbide aggregation processes. In [24], it was shown that the addition of tungsten to steel alloyed with Cr and Mo increases the ultimate strength at high temperatures by preventing the recovery of dislocations at tempering above 650 °C, which leads to a reduction in the size of $Me_{23}C_6$ carbides.

Recently, materials capable of resisting complex thermal, mechanical, chemical and electromagnetic stresses have been in demand [25,26]. This often requires the aggregation of several materials, which is usually accompanied by several problems in combining

them into a compact material. A brief enumeration of these problems in obtaining multi-compartment composites can be made as follows: physical and chemical incompatibility; high-stress concentration at the interface due to strong mismatch between thermal and mechanical properties; insufficient wetting or high mutual reactivity, etc., [27–29]. One of the possible solutions enabling the production of such composite materials is using hybrid technologies combining various manufacturing approaches. For example, the hybrid technology of electron-beam additive manufacturing (EBAM), including simultaneous or programmed feeding of wire and powder filaments, is a modern technology of additive manufacturing that makes it possible to produce components from metal-ceramic composites with a specified microstructure [30–32]. The authors of [30] discuss the mutual wettability of the added powder and matrix material during hybrid composite production by EBAM, which together give improved results in mechanical and tribological tests. At EBAM of aluminum alloy AA5154 with the addition of Mo powder [31], areas of unreacted Mo appear, as well as a large number of Al/Mo intermetallic precipitates, which caused high values of microhardness, as well as increased wear resistance of the material.

The aim of the present work is to study the microstructure and mechanical characteristics of composites with a matrix of heat-resistant high-alloy steel and two types of reinforcing particles: tungsten particles (W) and tungsten carbide + nickel (WC(Ni)). This composite was synthesized for the first time in the present work by a hybrid powder-wire method of electron-beam additive manufacturing.

2. Materials and Methods

The study focused on fabricating and characterizing composite steel samples reinforced with tungsten (W) and tungsten carbide (WC(Ni)) particles. The base material utilized was a 1-mm-diameter wire of 401S45 steel grade (ESAB Corporate, Gothenburg, Sweden), whose chemical composition (wt.%) included 86.9% Fe, 9.24% Cr, 3.02% Si, 0.44% C, and 0.4% Mn. The composite structure was created by alternately depositing layers of this steel wire and a reinforcing powder mixture of W and WC(Ni) (Highly pure chemicals (HPC), Moscow, Russia) in a 1:1 mass ratio. The process began by building up nine initial layers of 401S45 steel wire on an AISI 304 (Figure 1a) stainless steel substrate, forming a foundational matrix. Subsequently, 0.3 g of the W+WC(Ni) powder mixture was evenly distributed over the workpiece using the powder feeder (ISPMS SB RAS, Tomsk, Russia) shown in Figure 1b. The next layer of 401S45 wire (Figure 1c) was then added, which caused partial melting of both the powder and the underlying steel layer, promoting the binding of the matrix and powder. This sequence—powder application followed by wire deposition—was repeated three times, with each layer achieving a thickness of 1 mm. The final composite specimen (Figure 1d) had dimensions of 72 × 36 × 9 mm^3, comprising discrete zones: a base steel matrix, an intermediate transition layer (not shown in Figure 1), and a top composite layer enriched with W+WC(Ni) particles.

For metallographic (OM) and SEM analysis, the sample in the cross section was cut as shown in Figure 1d and prepared via standard metallographic techniques. This involved sequential grinding with abrasive papers (SiC) of progressively finer grit (14/10, 3/2, and 1/0), followed by polishing with diamond pastes. Chemical etching was performed using a reagent composed of 0.008 kg $CuSO_4$, 0.04 L H_2O, and 0.04 L HCl to reveal microstructural features. The etched surfaces were examined using an Altami Met 1S (Altami Ltd., St. Petersburg, Russia) optical microscope and an Olympus Lext OLS4100 (Olympus Corporation, Tokyo, Japan) confocal laser microscope for macro- and microstructural observations. High-resolution imaging and elemental analysis were conducted via scanning electron microscopy (SEM) on a Thermo Fisher Scientific Apreo S LoVac microscope (Thermo Fisher Scientific Inc., Waltham, MA, USA) equipped with an energy-dispersive

spectrometer (EDS). Local areas of the composite material ('TEM sample' in Figure 1d) were analyzed by transmission electron microscopy (TEM) Jeol 2100 (Jeol, Tokyo, Japan). The particle size in the composite layers was quantified using the secant method on TEM images. Phase composition was determined through X-ray diffraction (XRD) analysis on a DRON8 (Burevestnik, St. Petersburg, Russia) diffractometer utilizing CoKα and CuKα radiation to identify crystalline phases and assess structural changes induced by the deposition process. Samples for XRD analysis were cut from three zones, as shown in Figure 1d.

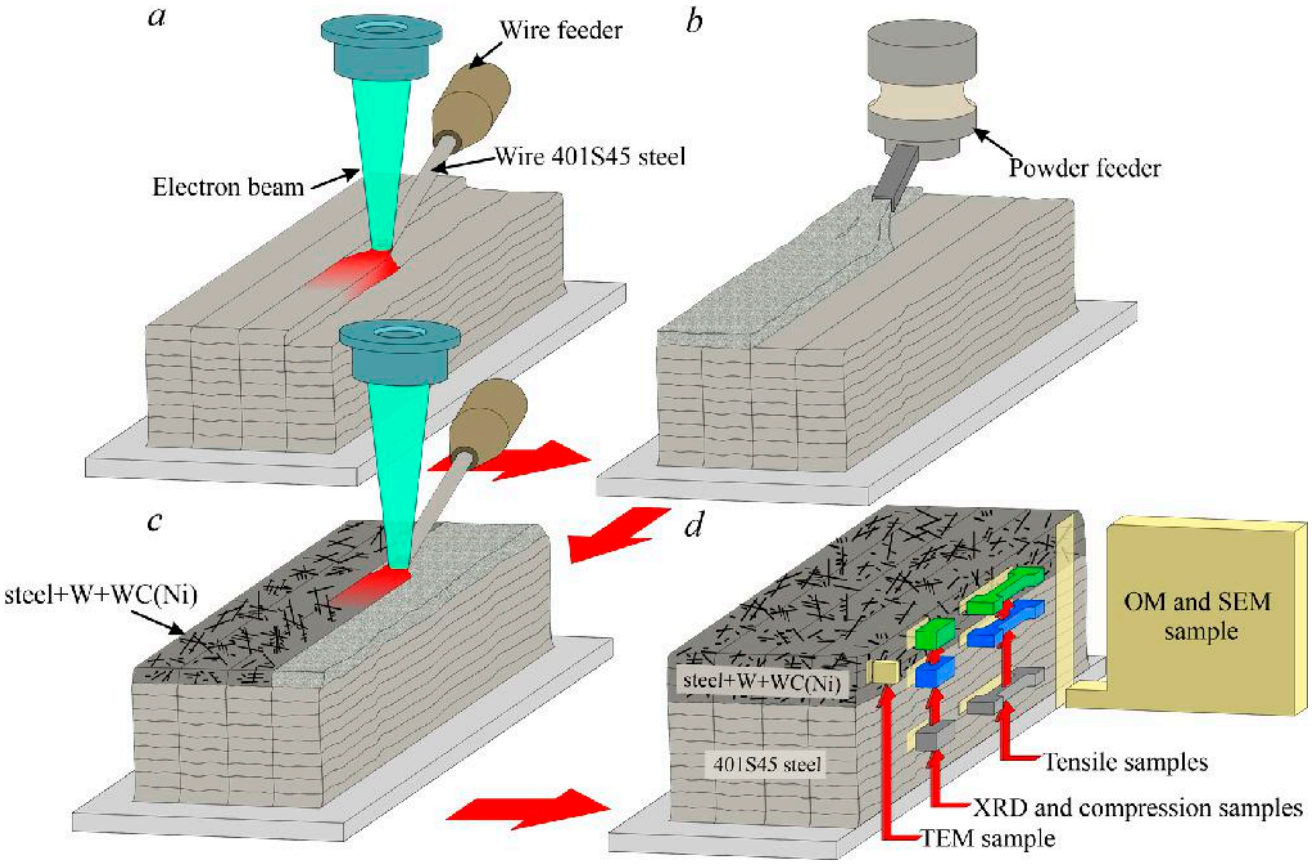

Figure 1. Printing scheme of steel+W+WC(Ni) composite produced by EBAM method and the scheme of cutting out samples for investigations. (**a**)—steel deposition, (**b**)—powder feeding, (**c**)—composite material formation, (**d**)—cutting scheme.

Mechanical properties were evaluated by measuring microhardness using a TBM 5215 A Tochline tester (Tochpribor, Moscow, Russia) under a 0.5 N load with a 10-s dwell time, providing insights into localized hardness variations across the composite. Microhardness measurements were performed on a cross-section of the composite sample. Uniaxial tensile and compression tests were performed at room temperature on a UTS-110M-100 (Test-system, Ivanovo, Russia) universal testing machine with a crosshead speed of 1 mm/min. Tensile ($12 \times 2.7 \times 1.5$ mm^3) and compression ($3 \times 3 \times 6$ mm^3) test specimens were cut from the matrix, transition and top layers along the layer deposition direction, as shown in Figure 1d. This approach enabled the assessment of mechanical behavior in different regions of the composite, accounting for variations in particle distribution matrix-particle interactions. The combination of structural and mechanical analyses aimed to correlate microstructural features with performance characteristics, providing a comprehensive understanding of the composite material's properties.

3. Results

3.1. Initial Powders W and WC(Ni)

The powder particles for the composite material were investigated by SEM and X-ray diffraction methods (Figure 2). The analysis of W (Figure 2b, PDF card number 00-004-0806) powder by SEM+EDS (Figure 2a) showed that besides W, there are also small amounts of oxygen and carbon. Moreover, oxygen is combined with tungsten in the WO_3 compound, which is observed from the diffractometry results (Figure 2b). Quantification of WO_3 (PDF card number 01-085-2460) from XRD data showed its content to be 4 ± 1.5 wt.%. The WC(Ni) powder was a mixture of two WC and Ni powders (Figure 2c). X-ray phase analysis revealed the WC (PDF card number 00-051-0939) and Ni (PDF card number 00-004-0850) phases (Figure 2d). The morphology of the powders used is, in all cases, represented by agglomerates of W, WC and Ni particles due to the method of production. The average size of the agglomerates of the tungsten powder was 20 ± 10 μm. For nickel and tungsten carbide powder: 45 ± 23 μm and 33 ± 12 μm, respectively.

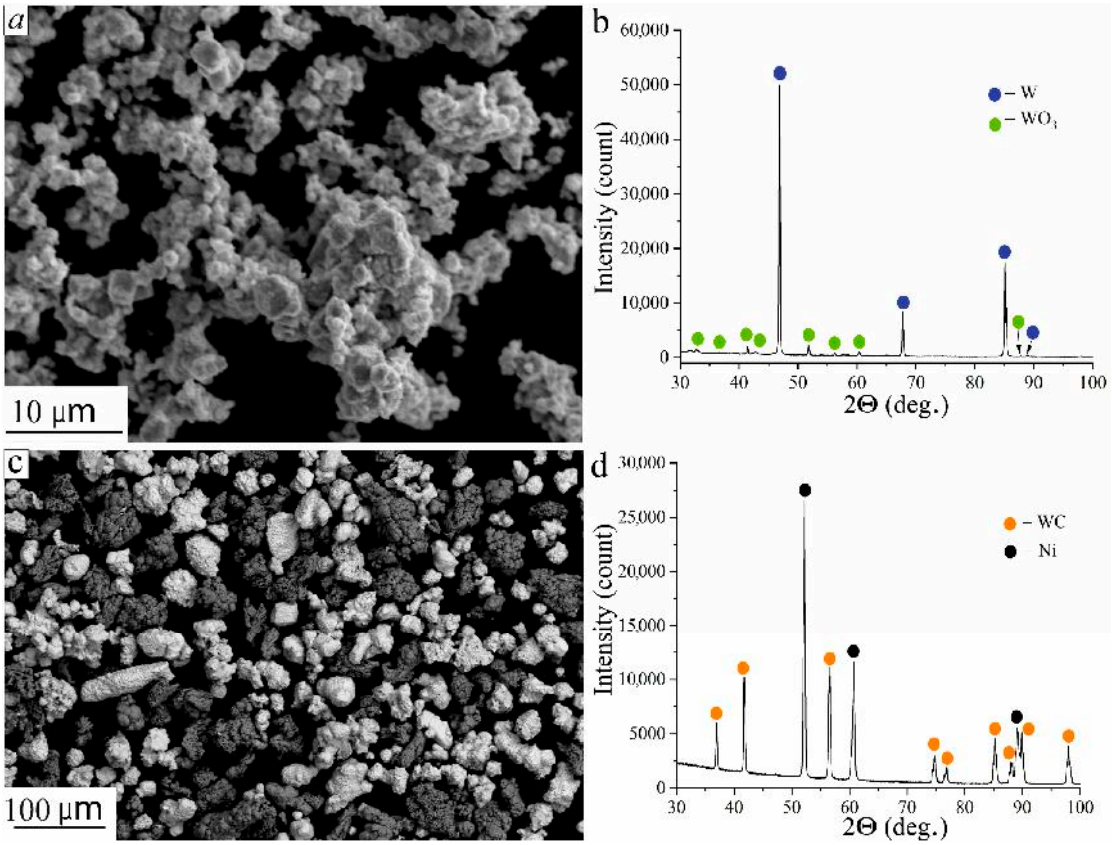

Figure 2. SEM SE images of W (**a**) and WC(Ni) (**c**) particles, the XRD patterns of W (**b**) and WC(Ni) (**d**) particles. The XRD imaging was performed using CoKa radiation.

3.2. Structure of Composite Steel+W+WC(Ni)

The optical microscopy image of the steel+W+WC(Ni) composite alloy in the cross-section is presented in Figure 3a, where several characteristic zones are highlighted: substrate; 401S45 steel layer; transition layer; steel+W+WC(Ni) composite layer. In the cross-section of the sample 401S45/(W+(WC(Ni)), a significant number of melt bath boundaries were formed during the EBAM of steel 401S45. The transition layer is expressed by a narrow gradient layer between the matrix and the composite layer (see Figure 3a). There are no macro-defects in the form of pores or cracks.

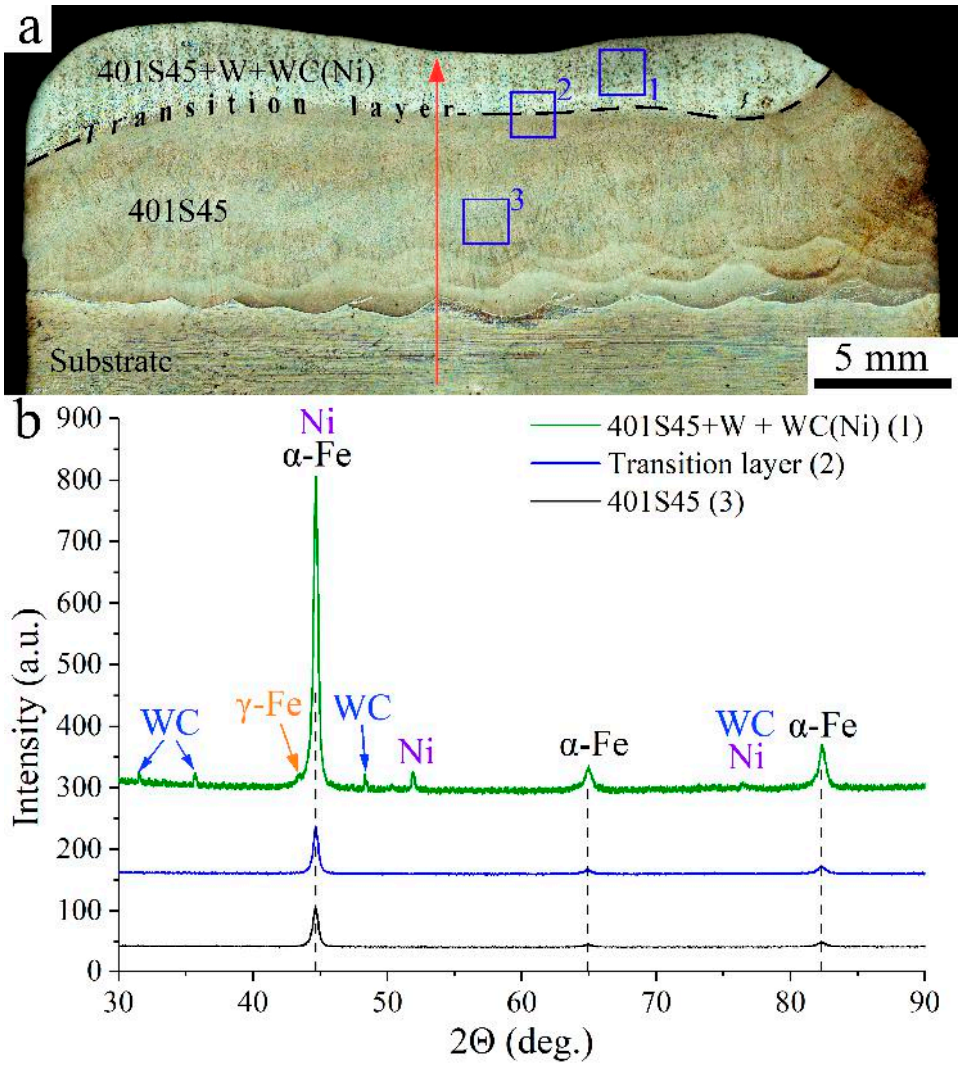

Figure 3. Macrostructure (**a**) and X-ray pattern (**b**) of the steel+W+WC(Ni) composite. The areas marked with numbers in the optical image are for XRD analysis in different regions of the composite. XRD imaging was performed using CuKα radiation. The arrow on "a" indicates the microhardness measurement line.

By XRD analysis, it was found that the steel+W+WC(Ni) composite consists of α-Fe (83.69 vol.%) (PDF card number 00-006-0696), Ni (6 vol.%) and WC carbide phase (10.31 vol.%) (see Figure 3b). The composite layer contains a minor proportion of γ-Fe (PDF card number 00-052-0513), whereas no γ-Fe was found in the main alloy and intermediate layer. The presence of γ-Fe is due to the dissolution of Ni in iron, which is a stabilizer for the austenitic phase of iron.

In steel 401S45 and the transition layer, there is a needle structure characteristic of martensite (Figure 4a,b). The composite matrix consists mainly of 82 at.% Fe, 9.7 at.% Cr, 0.09 at.% Mn and 7.5 at.% Si (Figure 4b, spectra 1 and 2), which corresponds to the initial composition of steel, taking into account the redistribution of chemical elements during melting and crystallization.

In the transition layer between steel and steel+W+WC(Ni) composite (Figure 4b), the needle structure becomes more pronounced. In addition to the elemental composition of the transition zone material, W is locally detected in the chemical elements of steel 401S45 (Figure 4b, spectrum 3). Fine particles of tungsten carbide WC with a size of 2.64 μm are also found along the grain boundaries (spectra 1-2, Figure 4c,d).

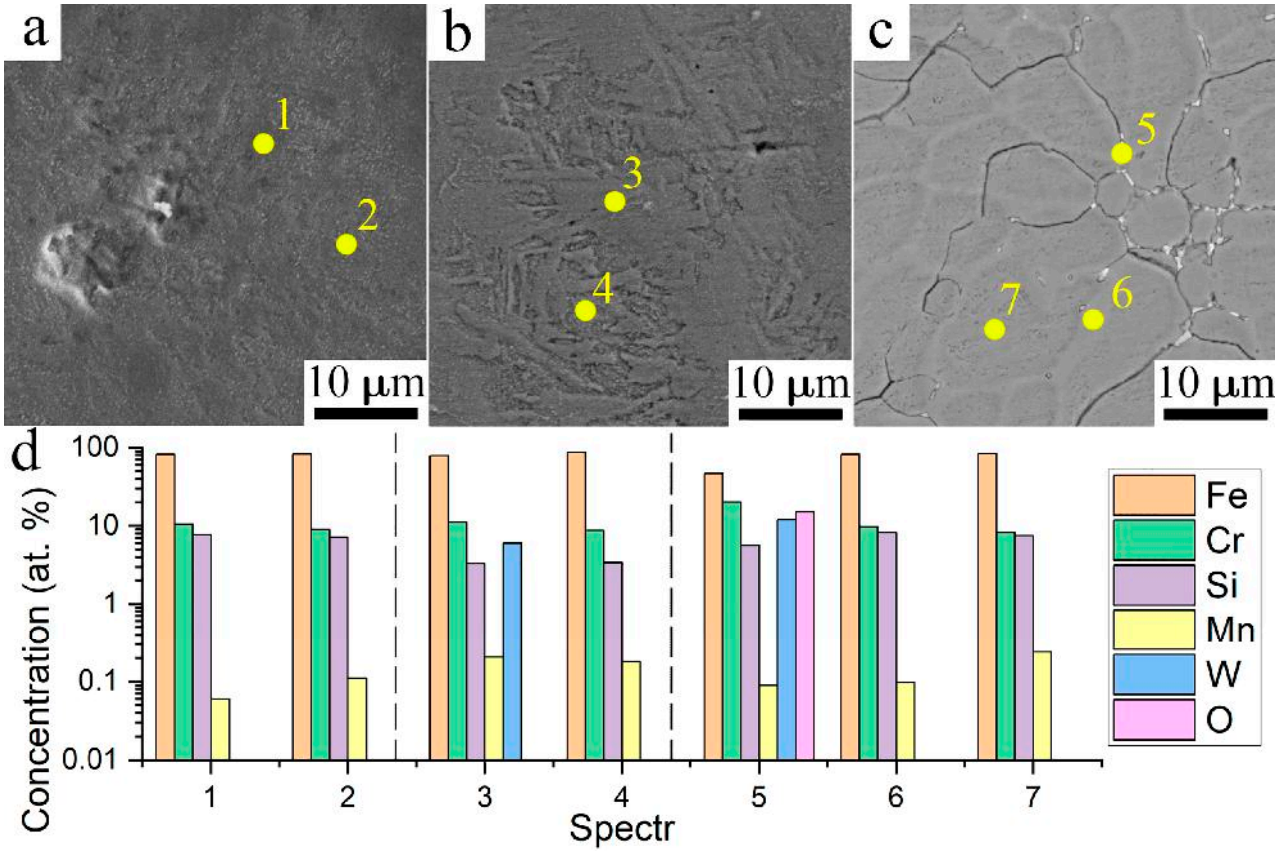

Figure 4. SEM images and elemental composition of the composite sample steel+W+WC(Ni): (**a**) layer of steel 401S45; (**b**) transition layer; (**c**) 401S45+W + WC(Ni) layer; (**d**) chemical composition at the points shown in (**a**–**c**).

In the composite layer steel+W+WC(Ni), an equiaxed grain structure with an average grain size of 8.6 ± 2.3 μm is formed, along the boundaries of which cracks are observed (Figure 4c). Tungsten and tungsten carbide particles are localized in cracks and in small amounts inside the grains (Figure 4c,d, spectrum 5). In the composite layer, the volume fraction of WC particles increases significantly compared to the base material and the intermediate layer. No tungsten was detected in the grain body by the EDS method (Figure 4b, spectra 6 and 7). According to XRD data (Figure 3b), the steel+W+WC(Ni) composite layer contains α-Fe (80.6 vol.%), Ni (6 vol.%), WC (10.3 vol.%) and a small fraction of γ-Fe (3 vol.%) (Figure 3b).

The TEM method found that the steel+W+WC(Ni) composite material has a multi-phase complex organized structure consisting of several main phases. Figure 5 shows the results of the TEM analysis. The brightfield image (Figure 5a) shows such structural elements as the matrix of the steel+W+WC(Ni) composite, particles of different morphologies and substructural elements in the form of stress fields at the particle boundaries and dislocations.

According to the results of the EDS analysis shown in Figure 5d, tungsten is present in both the composite matrix and particles. Analysis of the micro-diffraction pattern (Figure 5a) obtained from the region marked in Figure 5a shows the presence of α-Fe, Cr_7C_3 and particles of Fe-Cr-W ternary composition. At the same time, as shown in the dark-field image, there are dislocations in the matrix phase in large numbers (Figure 5b, shown by arrows). The ternary Fe-Cr-W particles are located both in the α-Fe grain body and at the boundaries.

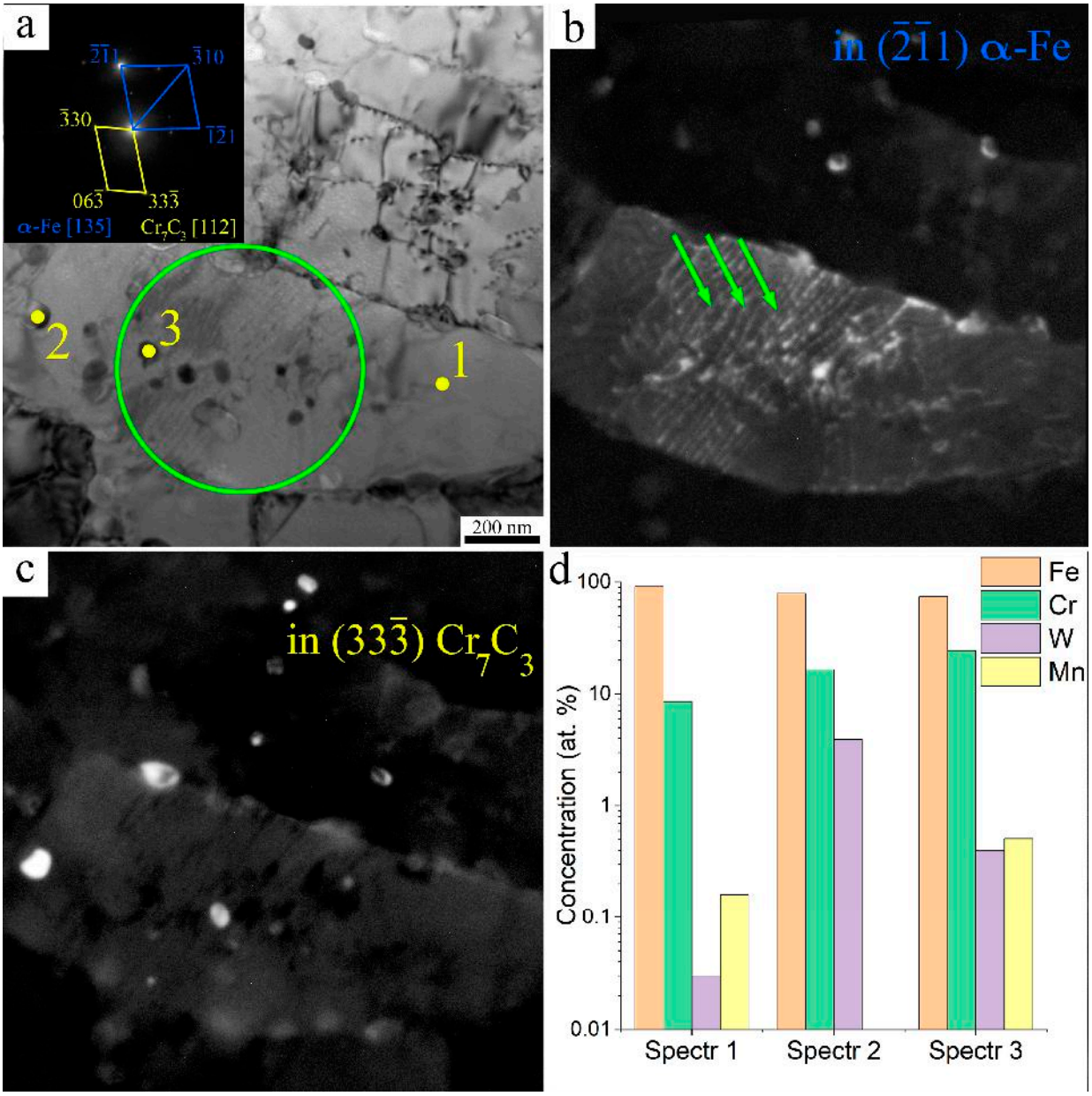

Figure 5. Results of TEM investigations of steel+W+WC(Ni) composite. (**a**) brightfield image and microdiffraction pattern, (**b**,**c**) darkfield images of matrix and particles, (**d**) EDS analysis obtained from the points marked in (**a**).

3.3. Mechanical Properties of Steel+W+WC(Ni) Composite

Microhardness measurements were carried out on the cross-section of the steel+W+WC(Ni) composite (Figure 6) along the line shown in Figure 3a. An increase in microhardness is observed in the transition from the substrate to the composite layer (Figure 6), which indicates gradient strengthening of the material. The specific microhardness values for 401S45 base alloy, transition layer and composite 401S45+W+WC(Ni) layer are 345 HV, 531 HV and 653 HV, respectively. This increase in microhardness compared to the initial 401S45 steel indicates an effective distribution of reinforcements in the composite structure, which may contribute to improved wear resistance and durability of the final product.

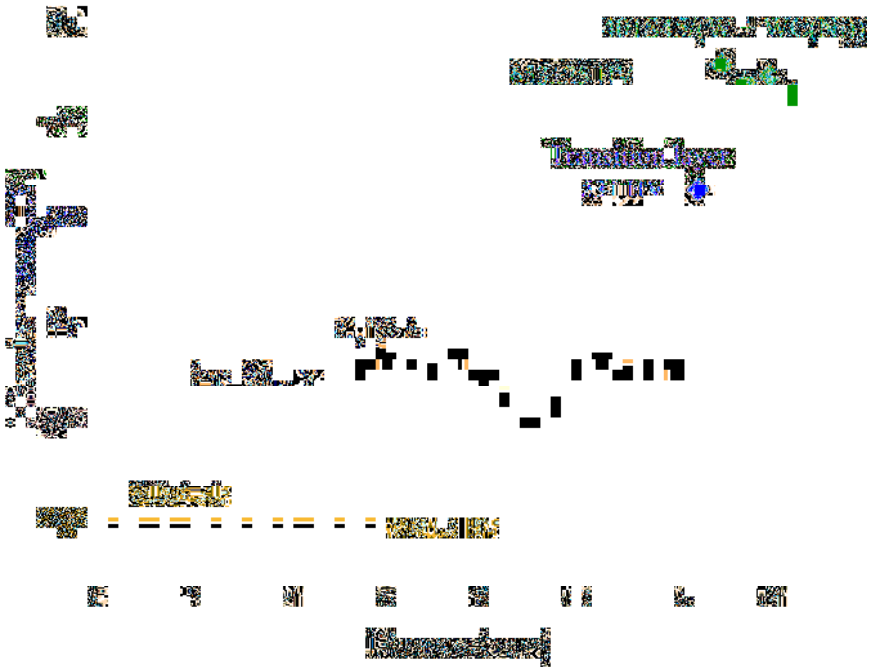

Figure 6. Microhardness measurement results of steel+W+WC(Ni) composite from the substrate to the top composite layer of the composite along the line shown in Figure 3a.

Uniaxial tensile tests of specimens cut from the main alloy zone and the intermediate layer (Figure 7a) demonstrate the ductile nature of the fracture. For specimens from the main alloy zone of 401S45, the ultimate strength and yield strength are approximately 1000 MPa and 650 MPa, respectively.

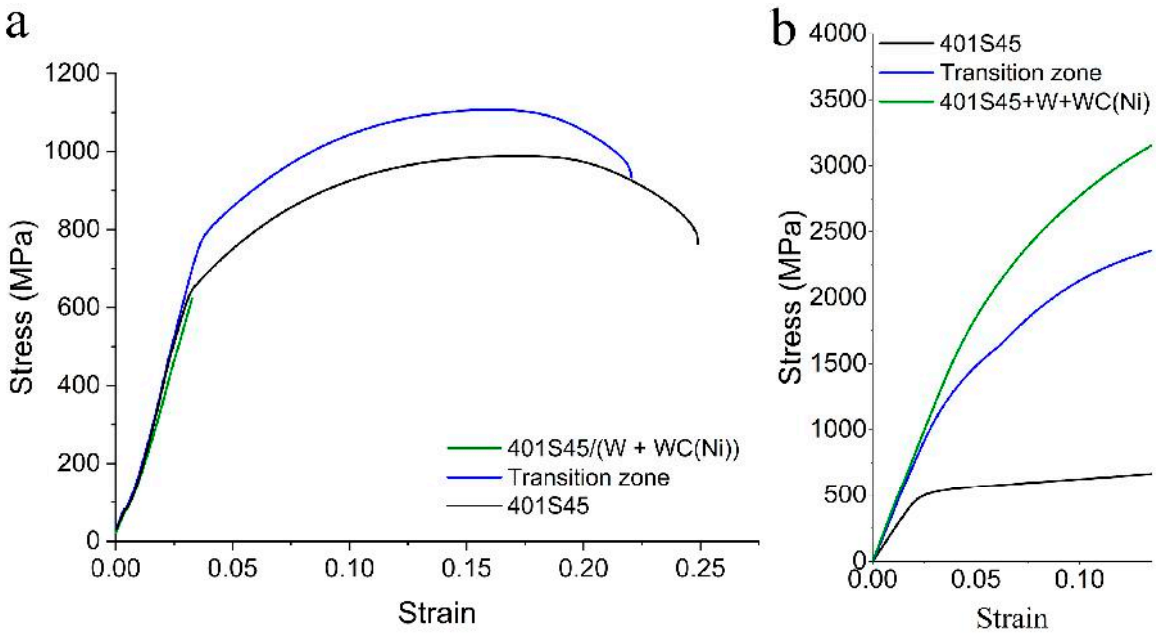

Figure 7. Stress-strain diagrams after tensile (**a**) and compression (**b**) tests.

For specimens from the transition zone steel—steel+W+WC(Ni), the ultimate strength and yield strength values increase to 1150 MPa and 830 MPa, respectively, which are 10% and 28% higher compared to the main alloy 401S45 (Figure 7a). This significant increase in mechanical properties can be attributed to the presence of tungsten carbides, which effectively prevent deformation of the matrix alloy, thereby increasing its strength

properties. At the same time, the relative elongation for the 401S45 zone and the transition zone remains comparable and averages 22%.

For the composite layer specimens, the strength limit of 620 MPa was observed (Figure 7a). The decrease in relative elongation up to 3% is due to the high volume fraction of brittle carbide particles located along the grain boundaries of the 401S45 alloy. Such a composite layer with a tungsten carbide content of about 10 vol.% can be classified as a typical metal-carbide composite, the mechanical properties of which are traditionally evaluated by compression rather than tension. This approach allows a more accurate characterization of the material behavior under load, considering the influence of brittle phases on the overall mechanical properties of the composite.

Compression tests were carried out for three structural zones: homogeneous matrix (401S45), transition layer, and composite layer (steel+W+WC(Ni)). The results revealed significant differences in the mechanical behavior of the zones investigated, highlighting the influence of the gradient structure on the strength distribution.

The 401S45 steel matrix exhibited a typical behavior for ductile materials: significant plastic deformation was observed in compression with the formation of a pronounced yield zone (Figure 7b, black line). YS in compression was 490 $\pm$ 25 MPa, which is consistent with the low concentration of hardening phases in this zone. The transition layer (Figure 7b, blue line) combining matrix 401S45 with initial inclusions of W+WC(Ni) showed an increase in strength by more than 100% compared to the pure matrix, YS was 1200 $\pm$ 60 MPa. Increasing the concentration of strengthening particles in the composite layer (steel+W+WC(Ni)) causes a further increase in the YS value up to 1720 $\pm$ 60 MPa (Figure 7b, green line).

4. Discussion

During additive manufacturing, there is a significant redistribution of carbon from tungsten carbide (WC) particles into the matrix α-Fe associated with melt formation. This diffusion mechanism significantly affects the matrix phase formation in the adjacent region from the carbide reinforcing particles since carbon is an austenite-forming element. It is assumed that a significant amount of diffused carbon passes into the α-Fe matrix in the form of embedded atoms, promoting the phase transformation α-Fe $\rightarrow$ γ-Fe in the forming composite layer (see Figure 3b). Additionally, the presence of nickel used in conjunction with WC particles also influences austenite stability since nickel is an austenite-forming element. For example, additional nickel alloying of high chromium steels allows for a certain chromium/nickel ratio to produce a fully austenitic structure at room temperature. This emphasizes the importance of controlling the alloying element content to achieve the desired microstructural characteristics of the material during additive manufacturing.

It is known that the ferrite-martensitic microstructure is prone to re-transformation to austenite during the melting of the powder layer [33]. This is due to the molten pool temperature exceeding the austenite transformation termination temperature due to the constant heat flow from the molten regions to the substrate [33]. Under such conditions, it can be expected that the formed austenite will again transform into martensite during rapid cooling. However, observations show that γ-Fe is not fixed in the main alloy and in the intermediate layer, and the phase composition consists predominantly of α-Fe. Nevertheless, a minor residual amount of austenite is observed in the composite layer (Figure 3b), which may be due to the presence of WC particles and nickel that slow down the complete transformation to α-Fe. This indicates complex interactions between carbide particles and matrix, which can influence phase transitions and stabilize certain phases on cooling.

An additional important observation is the absence of Me_3C-type carbides formed because of the interaction between iron and tungsten carbide WC. This can be attributed

to the positive effect of the addition of tungsten, which, due to its low diffusion mobility, slows down the kinetics of the formation of such carbides [21,22]. Thus, the introduction of WC into the matrix improves the stability of the phase composition of the material, preventing undesirable phase transformations and preserving the structural integrity of the reinforcing particles.

Microstructural analysis revealed a partial distribution of tungsten-containing particles, which helped to limit plastic deformation. The composite layer (steel+W+WC(Ni)) showed a maximum compressive strength (YS) exceeding that of the matrix by more than 300%, which was 1720 ± 60 MPa (Figure 7b, green line). The high concentration of W and WC(Ni) created a rigid skeleton (Figure 4c) that effectively redistributed the load. It is likely that in compression, the failure was localized, limited to the zones between the reinforcing particles, whereas in tensile tests, this layer performed the worst due to brittle fracture (Figure 7a, green line) at the matrix-strengthening phase interfaces. This contradiction emphasizes the anisotropy of the properties of gradient systems: high compressive strength is due to the resistance of the particles to shear deformations, whereas tensile strength is dominated by stress concentrators around the same inclusions.

The data obtained confirms that the gradient structure allows the plasticity of the matrix to be combined with the high compressive strength of the composite layer. However, the opposite pattern in tension indicates the need to optimize the interfaces between the phases to reduce brittleness. It is likely that the introduction of intermediate layers with a smooth W+WC(Ni) concentration gradient could soften the stress transition and improve the tensile properties without losing them in compression.

5. Conclusions

The microstructure and mechanical characteristics of a composite alloy based on steel 401S45 obtained by wire electron-beam additive manufacturing with the introduction of W+WC(Ni) powders during printing were investigated in this work. The steel+W+WC(Ni) composite alloy is characterized by a gradient structure consisting of a 401S45 base alloy, a steel—steel+W+WC(Ni) intermediate layer and a steel+W+WC(Ni) composite layer. Based on the research performed, the following conclusions can be drawn:

1. Microhardness values increase from 345 to 653 HV as one moves away from the substrate to the composite layer.

2. The composite layer (steel+W+WC(Ni)) shows high compressive strength (1720 ± 60 MPa) compared to unmodified steel, which is achieved due to a rigid framework of particles redistributing the load, whereas brittle fracture prevails in tension due to stress concentration at the phase boundaries.

Based on the obtained results, it is assumed that the addition of W+WC(Ni) powders into the surface layer of 401S45 steel by electron beam additive manufacturing will have a beneficial effect on the tribological properties of the resulting composite material, which will be discussed in detail in the next paper. This carries great potential to produce iron-based components with exceptional performance.

Author Contributions: Conceptualization, A.Z., A.V. and N.S. (Nikolai Savchenko); methodology, A.Z., A.V. and D.G.; formal analysis, A.Z., A.C. and N.S. (Nikolai Savchenko); investigation, A.V., A.Z., D.G., N.S. (Nikolay Shamarin), A.P. and N.S. (Nikolai Savchenko); resources, E.K.; writing—original draft preparation, A.V., A.Z., K.K. and N.S. (Nikolai Savchenko); writing—review and editing, A.V., A.Z. and N.S. (Nikolai Savchenko); visualization, A.V., A.Z., D.G., N.S. (Nikolay Shamarin), A.P. and N.S. (Nikolai Savchenko); supervision, A.V. and A.Z.; project administration, A.V. and A.Z.; funding acquisition, A.V. and A.Z. All authors have read and agreed to the published version of the manuscript.

Funding: This work was performed according to the Government research assignment for ISPMS SB RAS, project FWRW-2024-0001.

Data Availability Statement: Data will be made available on request.

Acknowledgments: The investigations have been carried out using the equipment of Share Use Centre "Nanotech" of the ISPMS SB RAS.

Conflicts of Interest: The authors declare no conflict of interest.

References

1. Bhowmik, A.; Kumar, R.; Beemkumar, N.; Kumar, A.V.; Singh, G.; Kulshreshta, A.; Mann, V.S.; Johnson Santhosh, A. Casting of particle reinforced metal matrix composite by liquid state fabrication method: A review. *Results Eng.* **2024**, *24*, 103152. [CrossRef]
2. Kumar Yadav Nartu, M.S.K.; Agrawal, P. Additive manufacturing of metal matrix composites. *Mater. Des.* 2025, *in press*. [CrossRef]
3. Tjong, S.C. Recent progress in the development and properties of novel metal matrix nanocomposites reinforced with carbon nanotubes and graphene nanosheets. *Mater. Sci. Eng. R Rep.* **2013**, *74*, 281–350. [CrossRef]
4. Radhamani, A.V.; Lau, H.C.; Ramakrishna, S. CNT-reinforced metal and steel nanocomposites: A comprehensive assessment of progress and future directions. *Compos. Part A Appl. Sci. Manuf.* **2018**, *114*, 170–187. [CrossRef]
5. AlMangour, B.; Grzesiak, D.; Yang, J.-M. Selective laser melting of TiC reinforced 316L stainless steel matrix nanocomposites: Influence of starting TiC particle size and volume content. *Mater. Des.* **2016**, *104*, 141–151. [CrossRef]
6. Enrici, T.M.; Dedry, O.; Boschini, F.; Tchuindjang, J.T.; Mertens, A. Microstructural and thermal characterization of 316L+WC composite coatings obtained by laser cladding. *Adv. Eng. Mater.* **2020**, *22*, 2000291. [CrossRef]
7. Yan, X.C.; Chen, C.Y.; Zhao, R.X.; Ma, W.Y.; Bolot, R.; Wang, J.; Ren, Z.M.; Liao, H.L.; Liu, M. Selective laser melting of WC reinforced maraging steel 300: Microstructure characterization and tribological performance. *Surf. Coat. Technol.* **2019**, *371*, 355–365. [CrossRef]
8. Gu, D.D.; Ma, J.; Chen, H.; Lin, K.; Xi, L. Laser additive manufactured WC reinforced Fe-based composites with gradient reinforcement/matrix interface and enhanced performance. *Compos. Struct.* **2018**, *192*, 387–396. [CrossRef]
9. Wang, J.D.; Li, L.Q.; Tao, W. Crack initiation and propagation behavior of WC particles reinforced Fe-based metal matrix composite produced by laser melting deposition. *Opt. Laser Technol.* **2016**, *82*, 170–182. [CrossRef]
10. Kang, N.; Ma, W.; Heraud, L.; El Mansori, M.; Li, F.; Liu, M.; Liao, H. Selective laser melting of tungsten carbide reinforced maraging steel composite. *Addit. Manuf.* **2018**, *22*, 104–110. [CrossRef]
11. Chen, H.; Gu, D.; Kosiba, K.; Lu, T.; Deng, L.; Xi, L.; Kühn, U. Achieving high strength and high ductility in WC-reinforced iron-based composites by laser additive manufacturing. *Addit. Manuf.* **2020**, *35*, 101195. [CrossRef]
12. Olumor, I.D.; Wisniewska, M.; Torresani, E.; Olevsky, E.A. Additive manufacturing and spark plasma sintering as effective routes for manufacturing of AISI 316L austenitic stainless steel—WC composites. *J. Mater. Res. Technol.* **2023**, *26*, 3234–3244. [CrossRef]
13. Zhang, T.; Yang, K.; Zhu, Z.; Xu, L.; Chen, G.; Fang, N.; Kou, S. Effect of Cr and W on microstructure and wear resistance of arc additive manufactured flux-cored wire for railway wheels. *J. Mater. Res. Technol.* **2024**, *30*, 3438–3447. [CrossRef]
14. Li, H.; Hu, Y.; Di, R.; Yuan, R.; Shi, C.; Lei, J. Effects of WC particles on microstructure and mechanical properties of 316L steel obtained by laser melting deposition. *Ceram. Int.* **2022**, *48*, 20388–20399. [CrossRef]
15. Varun Kumar, K.; Kalyan Phani, M. Microstructural and mechanical characterization of parallel layered WC- NiCr weld overlay on 080 M40 steel substrate prepared using additive manufacturing. *Mater. Today Proc.* **2022**, *67*, 501–506. [CrossRef]
16. Kang, N.; Ma, W.; Lib, F.; Liao, H.; Liu, M.; Coddet, C. Microstructure and wear properties of selective laser melted WC reinforced 18Ni-300 steel matrix composite. *Vacuum* **2018**, *154*, 69–74. [CrossRef]
17. Yu, X.; Bai, X.; Shi, X.; Zhou, X.; Zhang, H. Microstructures and properties of wire and arc additively manufactured steel matrix composites with addition of WC by gravity-driven side powder feeding. *J. Manuf. Process.* **2022**, *81*, 236–249. [CrossRef]
18. Farahmand, P.; Kovacevic, R. Corrosion and wear behavior of laser cladded Ni–WC coatings. *Surf. Coat. Technol.* **2015**, *276*, 121–135. [CrossRef]
19. Liu, W.; Gao, D. Microstructure and wear of Ni-WC hardfacing used for steel-body PDC bits. *Int. J. Refract. Met. Hard Mater.* **2021**, *101*, 105683. [CrossRef]
20. Tahaei, A.; Bagheri Vanani, B.; Abbasi, M.; Arizmendi-Morquecho, A. A different attempt to investigate the influence of PTA parameters on microstructure evolution and mechanical characteristics of nickel base powder (Ni-WC) deposited tool steel. *J. Mater. Res. Technol.* **2023**, *27*, 7970–7985. [CrossRef]
21. Ding, H.; Yuan, Z.; Liu, T.; Chen, L.; Zhou, Y.; Cao, Y.; Cao, F.; Luo, R.; Cheng, X. Microstructure and high-temperature tensile behavior of modified H13 steel with the addition of tungsten, molybdenum, and lowering of chromium. *Mater. Sci. Eng. A* **2023**, *866*, 144655. [CrossRef]

22. Won, Y.J.; Kwon, Y.J.; You, J.S.; Park, S.S.; Cho, K.S. Role of W addition in reducing heat checking and enhancing the mechanical properties of hot work tool steel. *J. Mater. Res. Technol.* **2023**, *24*, 3413–3422. [CrossRef]
23. Xiang, S.; Wu, R.; Li, W.; Hu, T.; Huang, S. Improved red hardness and toughness of hot work die steel through tungsten alloying. *J. Mater. Eng. Perform.* **2021**, *30*, 6146–6159. [CrossRef]
24. Hong, S.G.; Lee, W.B.; Park, C.G. The effects of tungsten addition on the microstructural stability of 9Cr–Mo Steels. *J. Nucl. Mater.* **2001**, *288*, 202–207. [CrossRef]
25. Matějíček, J.; Boldyryeva, H.; Brožek, V.; Sachr, P.; Chráska, T.; Pala, Z. W–steel and W–WC–steel composites and FGMs produced by hot pressing. *Fusion Eng. Des.* **2015**, *100*, 364–370. [CrossRef]
26. Bolt, H.; Barabash, V.; Krauss, W.; Linke, J.; Neu, R.; Suzuki, S.; Yoshida, N.; Team, A.U. Materials for the plasma-facing components of fusion reactors. *J. Nucl. Mater.* **2004**, *329–333*, 66–73. [CrossRef]
27. Odegard, B.C.; Cadden, C.H.; Watson, R.D.; Slattery, K.T. A review of the US joining technologies for plasma facing components in the ITER fusion reactor. *J. Nucl. Mater.* **1998**, *258–263*, 329–334. [CrossRef]
28. Merola, M.; Akiba, M.; Barabash, V.; Mazul, I. Overview on fabrication and joining of plasma facing and high heat flux materials for ITER. *J. Nucl. Mater.* **2002**, *307–311*, 1524–1532. [CrossRef]
29. Hamilton, N.R.; Wood, J.; Galloway, A.; Robbie, M.B.O.; Zhang, Y. The metallurgy, mechanics, modelling and assessment of dissimilar material brazed joints. *J. Nucl. Mater.* **2013**, *432*, 42–51. [CrossRef]
30. Filippov, A.V.; Khoroshko, E.S.; Shamarin, N.N.; Savchenko, N.L.; Moskvichev, E.N.; Utyaganova, V.R.; Kolubaev, E.A.; Smolin, A.Y.; Tarasov, S.Y. Characterization of gradient CuAl–B4C composites additively manufactured using a combination of wire-feed and powder-bed electron beam deposition methods. *J. Alloys Compd.* **2021**, *859*, 157824. [CrossRef]
31. Zykova, A.; Chumaevskii, A.V.; Vorontsov, A.; Shamarin, N.; Panfilov, A.; Knyazhev, E.; Moskvichev, E.; Gurianov, D.; Savchenko, N.; Kolubaev, E.; et al. Microstructural evolution of AA5154 layers intermixed with Mo powder during electron beam wire-feed additive manufacturing (EBAM). *Metals* **2022**, *12*, 109. [CrossRef]
32. Utyaganova, V.R.; Chumaevskii, A.V.; Shamarin, N.N.; Moskvichev, E.N.; Vorontsov, A.V.; Gurianov, D.A.; Knyazhev, E.O.; Savchenko, N.L. Regularities of structure formation and properties of composite materials based on aluminum–manganese bronze produced by electron beam additive manufacturing with the addition of iron, nickel, and tungsten powders during printing. *Russ. Phys. J.* **2023**, *65*, 1584–1591. [CrossRef]
33. Holzweissig, M.J.; Taube, A.; Brenne, F.; Schaper, M.; Niendorf, T. Microstructural characterization and mechanical performance of hot work tool steel processed by selective laser melting. *Metall. Mater. Trans. B* **2015**, *46*, 545–549. [CrossRef]